

# All-Conjugated Polymer Core–Shell and Core–Shell–Shell Particles with Tunable Emission Profiles and White Light Emission

Bastian Haehnle, Philipp A. Schuster, Lisa Chen, and Alexander J. C. Kuehne\*

Future applications of conjugated polymer particles (CPP) in medicine, organic photonics, and optoelectronics greatly depend on high performance and precisely adjustable optical properties of the particles. To meet these criteria, current particle systems often combine conjugated polymers with inorganic particles in core–shell geometries, extending the possible optical characteristics of CPP. However, current conjugated polymer particles are restricted to a single polymer phase composed of a distinct polymer or a polymer blend. Here, a synthetic toolbox is presented that enables the synthesis of monodisperse core–shell and core–shell–shell particles, which consist entirely of conjugated polymers but of different types in the core and the shells. Seeded and fed-batch dispersion polymerizations based on Suzuki–Miyaura-type cross-coupling are investigated. The different approaches allow accurate control over the created interface between the conjugated polymer phases and thus also over the energy transfer phenomena between them. This approach opens up completely new synthetic freedom for fine tuning of the optical properties of CPP, enabling, for example, the synthesis of individual white light-emitting particles.

dreds of nanometers and up to several microns.<sup>[5–9]</sup> Alternatively, bottom-up dispersion polymerization can be employed, where particles form during polymerization leading to more homogeneous and uniform particles with tunable sizes from  $\approx 100$  nm to the micrometer range.<sup>[10–12]</sup> Such all-conjugated polymer particles are superior to their dye-doped dielectric polymer counterparts regarding their stability towards photobleaching,<sup>[13]</sup> their absorption cross-section,<sup>[14,15]</sup> and optical gain.<sup>[16,17]</sup> Moreover, core–shell particles with inorganic core particles and conjugated polymer shells have given access to novel properties beyond the limits of organic materials.<sup>[18]</sup> Among these, silica microparticles@CPP core–shell particles have been reported as whispering gallery mode resonators,<sup>[19]</sup> magnetite nanoparticles@CPP have been reported as magnetic resonance imaging probes,<sup>[20]</sup> and plasmonic gold nanoparticles@CPP have

## 1. Introduction

Conjugated polymer particles (CPP) represent a powerful class of materials with applications ranging from colloidal, self-assembled photonic devices<sup>[1,2]</sup> to biomedical vehicles for imaging and therapeutic utilization.<sup>[3,4]</sup> Conjugated polymer particles can be produced in top-down processes by dispersing conjugated polymers in mini-emulsions or hot injection procedures, where polymer particles crash out and can be harvested as polydisperse products with diameters in the range of hun-

been presented for photodynamic therapy<sup>[21]</sup> or photoacoustic imaging probes.<sup>[22,23]</sup> Core–shell particles produced from conjugated polymer in the core as well as in the shell (CPP@CPP) are not accessible using top-down processing, because the solvents used for applying the shell-polymer would dissolve the core polymer. By contrast, bottom-up processing using for example a seeded dispersion polymerization could in principle give access to CPP@CPP particles. However, so far, this approach has not been applied to all-conjugated polymer core–shell particles. Due to unfavorable Flory–Huggins interaction parameters and incompatible surface energies in CPP@CPP syntheses, secondary nucleation of individual shell-particles often occurs preferentially over condensation of the shell polymer onto the core particles.<sup>[24–27]</sup> This “demixing” leads to core–shell particles with heterocoagulated “bumpy” shells<sup>[28,29]</sup> in the best case and separate core-polymer particles and shell-polymer particles in the worst case, which is probably why the seeded dispersion polymerization protocol has not been applied to CPP@CPP.

Such narrowly dispersed and uniform CPP@CPP particles would present interesting materials that enable controlled energy transfer pathways within particles and multimodal or white light emission from individual particles with applications ranging from optoelectronics to photonics and biomedical imaging.<sup>[30–33]</sup> However, the lack of synthetic strategies yielding high quality conjugated polymer core–shell particles obviates these high-potential applications.

B. Haehnle, P. A. Schuster, L. Chen, Prof. A. J. C. Kuehne  
Institute of Organic and Macromolecular Chemistry  
Ulm University  
Albert-Einstein-Allee 11, Ulm 89081, Germany  
E-mail: alexander.kuehne@uni-ulm.de

Prof. A. J. C. Kuehne  
DWI – Leibniz-Institute for Interactive Materials  
Forckenbeckstraße 50, Aachen 52074, Germany

 The ORCID identification number(s) for the author(s) of this article can be found under <https://doi.org/10.1002/smll.202101411>.

© 2021 The Authors. Small published by Wiley-VCH GmbH. This is an open access article under the terms of the Creative Commons Attribution-NonCommercial-NoDerivs License, which permits use and distribution in any medium, provided the original work is properly cited, the use is non-commercial and no modifications or adaptations are made.

DOI: 10.1002/smll.202101411

Here, we present a fed-batch process, which allows us to grow a conjugated polymer shell in situ during dispersion polymerization onto previously nucleated core particles of a different conjugated polymer. We compare the fed-batch process to CPP@CPP particles formed by the seeded dispersion polymerization protocol. We investigate the sharpness of the interface of the different conjugated polymers and characterize the energy transfer properties resulting from the structure of the boundary region. We demonstrate that our concept can be generalized to a variety of conjugated polymers and we showcase the versatility by producing core-shell-shell particles of three different conjugated polymers.

## 2. Results and Discussion

A variety of commercially available monomers with halide and boronic acid or boronic ester groups can be employed in Suzuki cross-coupling polymerization.<sup>[34]</sup> Typically, Suzuki–Miyaura dispersion polymerization is performed in *n*-propanol, which is a solvent for all partaking monomers, catalyst, stabilizers, and base, but it is a nonsolvent for the resulting conjugated polymers, giving access to monodisperse CPP with diameters from a few hundred nanometers to about 1  $\mu\text{m}$ .<sup>[10]</sup> Suzuki–Miyaura dispersion polymerization provides access to CPP from a wide variety of conjugated polymers with different absorption profiles and emission colors as well as of controllable particle size, precisely tailored to the desired application.

Recently, we reported a fed-batch dispersion polymerization based on Heck cross-coupling, where a part of the reactants are introduced to start the reaction and the remainder is slowly fed to the reaction mixture at a constant rate using a syringe pump.<sup>[35]</sup> Continuous feeding of reactants prevents secondary nucleation, which is otherwise a problem in dispersion polymerizations with high monomer loading, enabling the synthesis of large conjugated polymer particles with diameters of up to 4  $\mu\text{m}$ .

To produce core-shell particles of different conjugated polymers in the core and in the shell we can now follow two approaches. First, we can perform a seeded dispersion polymerization, where we first produce the core particle in an individual dispersion polymerization step. After purification, the particles are applied as nucleation sites during a seeded dispersion polymerization of the shell polymer (see **Figure 1a**: seeded and **Figure S1** (Supporting Information)). Second, we can synthesize the core particles by dispersion polymerization and after the synthesis is complete we then feed the monomers for producing the shell to the same reactor (see **Figure 1a**: fed-batch and **Figure S1** (Supporting Information)).

The “seeded” approach requires careful redispersion of the seeds and prevention of seed-aggregation in the reaction mixture, as otherwise polydisperse CPP are obtained. Another major challenge is inhibition of secondary nucleation of the shell polymer, which otherwise leads to bidisperse or polydisperse particles (see **Figure S2** in the Supporting Information). Secondary nucleation can partly be compensated for by careful adjustment of the seed and shell monomer concentrations.<sup>[36]</sup> By contrast, the fed-batch dispersion polymerization is less susceptible to these problems as it is performed in a single batch and the concentration of the shell monomers and reactants is always starved.<sup>[37,38]</sup> Purification and redispersion of the core particles are therefore not required.

In this study we first compare particles composed of poly(9,9-dioctylfluorene-*alt*-triphenylamine) (F8TPA) and poly(9,9-dioctylfluorene-*co*-di-3-hexylthiophene-benzothiadiazole) (F8-T/BT) due to their spectrally well separated emission colors (see **Figure 1b** and **Figure 2a,b**). To produce the core particles and shells in either approach, we employ typical Suzuki–Miyaura dispersion polymerization, which is well studied and offers a large number of applicable monomers. We use *n*-propanol as solvent, tetrakis(triphenyl-phosphine)-palladium(0) (Pd(PPh<sub>3</sub>)<sub>4</sub>) as catalyst, potassium *tert*-butoxide (KOtBu) as base, and a mixture of Triton X-45 and poly(vinylpyrrolidone-*co*-vinyl acetate) ( $M_n \approx 50$  kDa) (PVPVA) as stabilizers.<sup>[10]</sup>

Monodispersity of the core particles is a prerequisite for monodisperse core-shell CPP@CPP in both methods. We present reaction conditions that result in monodisperse CPP for both the copolymer F8TPA as well as for the terpolymer F8-T/BT (see Experimental Section in the Supporting Information). The monodispersity of CPP synthesized via dispersion polymerization strongly depends on a simultaneous nucleation process, which does not seem to be affected by the presence of three reacting monomers. Monodispersity of F8-T/BT and F8TPA particles is easily demonstrated macroscopically, by their characteristic iridescence upon drying (see **Figure 1c**, insets). The iridescence is an effect of colloidal self-assembly into opaline photonic crystals. Investigation using scanning electron microscopy (SEM) enables determination of the particle diameters and again reveals that they readily assemble into hexagonal crystals (see **Figure 1c**). We can vary the F8-T/BT particle diameter between 400 and 600 nm, by adjusting the monomer concentration from 10.5 to 14.5 mmol L<sup>-1</sup>. In the same manner, we can also set the diameters of F8TPA particle between 300 and 500 nm by varying the monomer concentration between 8.0 and 10.5 mmol L<sup>-1</sup> (see **Figure 1d**).

Before investigating the core shell approach, we first test the fed-batch method and stick to F8-T/BT in the core as well as in the shell. We prepare the cores using 11.5 mmol L<sup>-1</sup> of monomers M1, M2, and M3 yielding seed particles with diameters of 550 nm as determined from aliquots taken from the reaction mixture. After 150 min, the core particles do not grow any further in their diameter and we start to feed the reaction mixture with 20.8 mmol L<sup>-1</sup> of M1, M2, and M3. The final F8-T/BT@F8-T/BT<sub>fb</sub> (fb subscript for fed-batch) particles are monodisperse with diameters of 810 nm (**Figure 1c**, middle and **Figure 1d**). Assured by these results, we repeat this approach and feed monomers M1 and M4 after F8-T/BT seed formation, to obtain F8-T/BT@F8TPA<sub>fb</sub> particles. It would be desirable to also have control over the thickness of the F8TPA shell. In this approach, we indeed observe that we can control the F8TPA shell thickness by tuning the amount of added monomers M1 and M4 (see **Figure 1f**). Furthermore, the fed-batch approach also delivers monodisperse particles, when the shell is made of a different polymer than the core as in our F8-T/BT@F8TPA<sub>fb</sub> particles (see **Figure 1e**, left). Precise control over the shell thickness should only be possible if the shell formation does not occur via heterocoagulation of small F8TPA particles, but via controlled condensation of individual polymer chains onto the F8-T/BT seed particles leading to controlled growth. To prove this mechanism, we track the particle diameter throughout the fed-batch dispersion polymerization. We take aliquots every 5–30 min

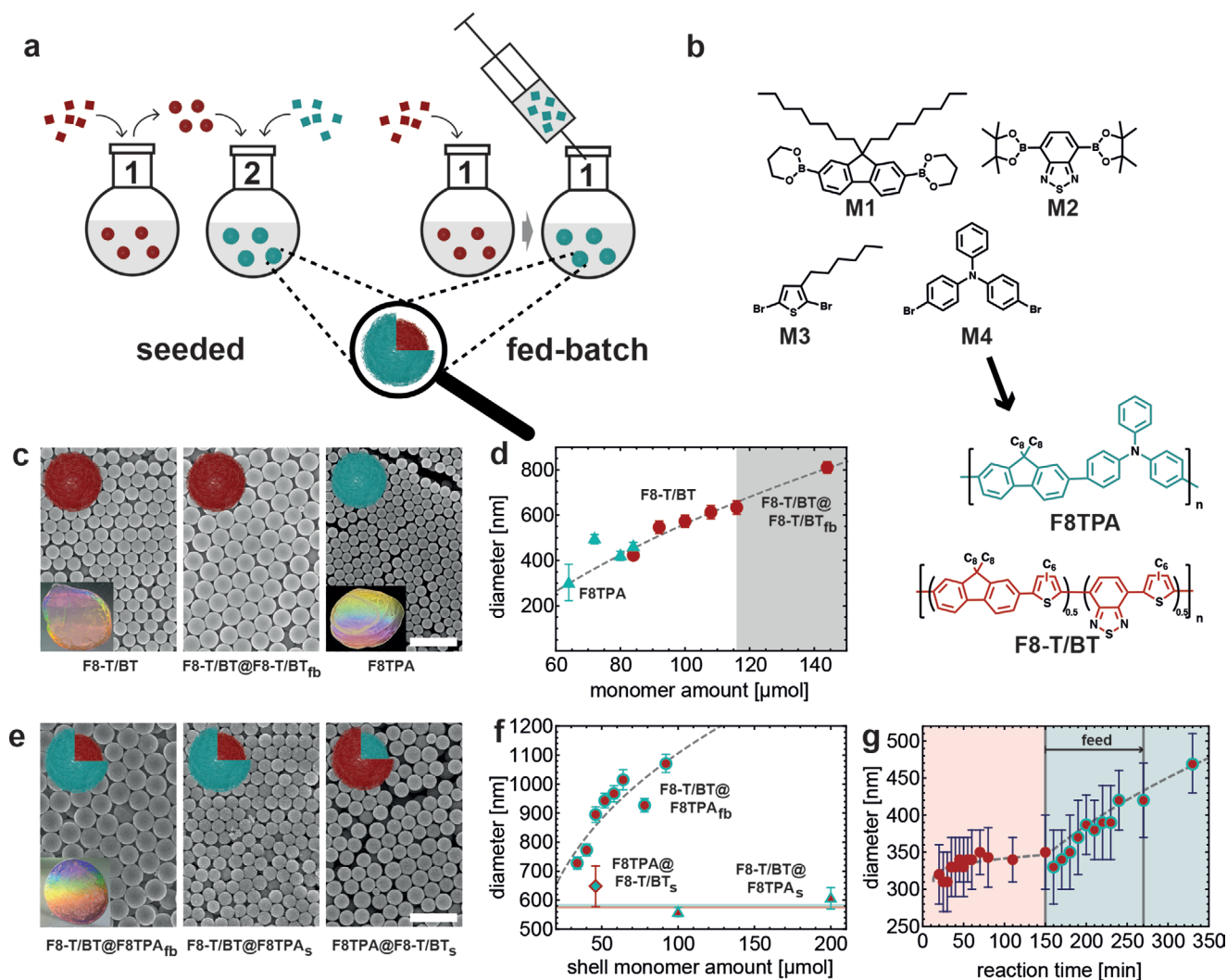


**Figure 1.** Synthesis of monodisperse core-shell CPP. a) Schematic illustration of the two different methods resulting in core-shell CPP. Left: Seeded dispersion polymerization, in which presynthesized CPP cores from a first batch are purified and used as seeds in a second reaction. Right: Fed-batch dispersion polymerization, in which the monomers and base for producing the shell polymer are fed in situ to the batch of the CPP core synthesis. b) Molecular structures of the monomers M1–M4 and resulting polymers F8TPA and F8-T/BT. c) SEM images of core CPP with schematic illustrations of the respective particle emission colors as inset in the upper left corner. Left: F8-T/BT particles. Inset shows the iridescence of drop-casted particles on a glass slide. Middle: Large F8-T/BT particles obtained by fed-batch dispersion polymerization. Right: F8TPA particles. Inset shows the iridescence of drop-casted particles on a glass slide. Scale bar is valid for all panels and represents 2  $\mu\text{m}$ . d) Diameters with standard deviation of F8TPA (blue) and F8-T/BT (red) core particles as a function of total monomer amount. The shaded area indicates the particle diameters only available via fed-batch dispersion polymerization. The dashed line is a guide to the eye. e) SEM images of core-shell CPP with schematic illustrations of a respective particle as inset in the upper left corner. Left: F8-T/BT@F8TPA<sub>fb</sub> particles. Inset shows the iridescence of drop-casted particles on a glass slide. Middle: F8-T/BT@F8TPA<sub>s</sub>. Right: F8TPA@F8-T/BT<sub>s</sub> particles. Scale bar is valid for all panels and represents 2  $\mu\text{m}$ . f) Diameters with standard deviation of core-shell particles as a function of total shell monomer amount. All core-shell particles are based on  $\approx 590$  nm F8-T/BT or F8TPA core particles represented by the red and blue horizontal line respectively. F8-T/BT@F8TPA<sub>fb</sub> particles are displayed as red/blue circles. F8-T/BT@F8TPA<sub>s</sub> particles are displayed as red/blue triangles. F8TPA@F8-T/BT<sub>s</sub> particles are displayed as blue/red diamond. g) Tracking of F8-T/BT@F8TPA<sub>fb</sub> particle diameters with standard deviation over time during fed-batch dispersion polymerization. Red shaded area indicates the F8-T/BT core growth. Blue shaded area indicates the particle growth caused by the F8TPA shell. The first 150 min correspond to a regular dispersion polymerization for the synthesis of F8-T/BT particles. From 150 to 270 min there is a continuous feed of monomers and base for the F8TPA shell. The reaction was allowed to continue until 330 min. The dashed lines follow the equation for diameter increase at constant feed.

and analyze the purified particles via SEM (see Figure 1g and Figure S3 (Supporting Information)). During synthesis of F8-T/BT core particles, the reaction mixture turns turbid within the first 5 min indicating the nucleation process. The nuclei grow to form particles within the following 15 min and reach their final diameter of 350 nm after about 50 min. After 150 min

we start feeding the F8TPA monomers (20.8 mmol L<sup>-1</sup>) over the course of 120 min and eventually let the reaction complete during an additional 60 min. During the F8TPA monomer feed, we observe a steady increase of the particle diameter, which represents controlled shell growth. However, the overall particle growth during shell growth is much slower compared to

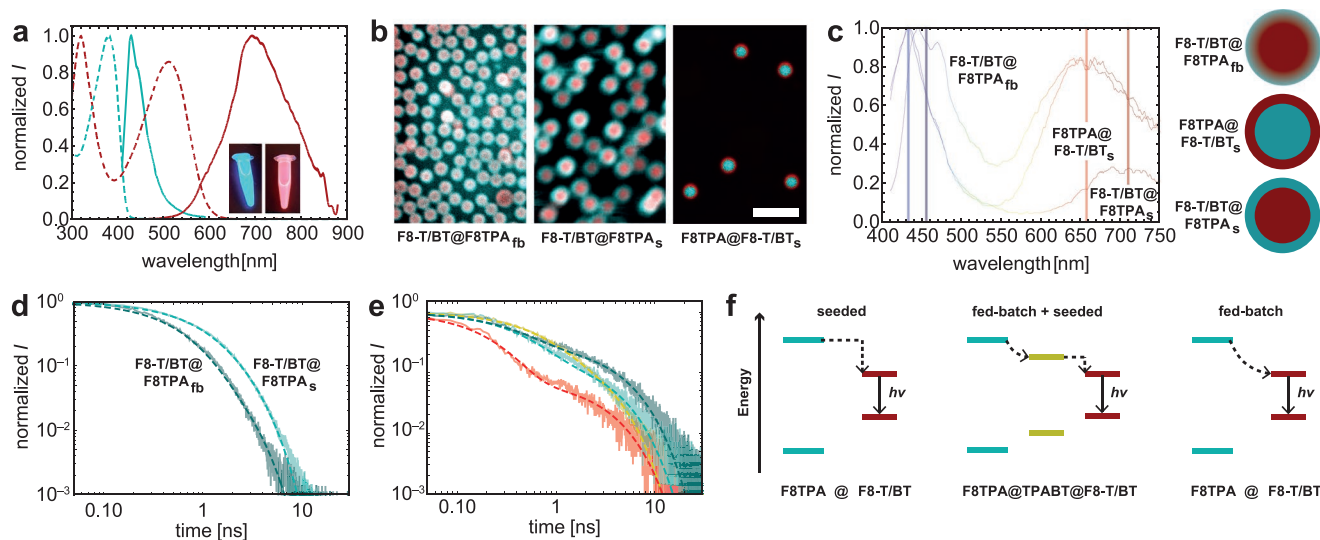


**Figure 2.** Optical characterization. a) Absorption spectra of solutions in THF (dashed lines) and fluorescence spectra of dispersions in *n*-propanol (solid lines) of F8TPA (cyan) and F8-T/BT (red) particles. Excitation wavelength  $\lambda_{\text{ex}} = 390$  nm. The inset shows photos of the fluorescence of dissolved F8TPA particles (left) and F8-T/BT particles (right) in THF at  $\lambda_{\text{ex}} = 365$  nm. b) Confocal laser scanning microscopy (CLSM) data of core-shell CPP. Left: F8-T/BT@F8TPA<sub>fb</sub>. Middle: F8-T/BT@F8TPA<sub>s</sub>. Right: F8TPA@F8-T/BT<sub>s</sub>. Scale bar represents 2  $\mu\text{m}$ . c) Fluorescence spectra of F8-T/BT@F8TPA<sub>fb</sub>, F8-T/BT@F8TPA<sub>s</sub>, and F8TPA@F8-T/BT<sub>s</sub> particle dispersions in *n*-propanol.  $\lambda_{\text{ex}} = 390$  nm. Vertical red and blue lines indicate the shifts in emission. Schematic illustration shows the different architectures and interfaces of the respective particles. d) Photoluminescence lifetime decay curves of the donor in F8-T/BT@F8TPA<sub>s</sub> (cyan) and F8-T/BT@F8TPA<sub>fb</sub> (darker cyan) particles. e) Photoluminescence lifetime decay curves of the acceptor F8-T/BT (red), F8-T/BT@F8TPA<sub>s</sub> (cyan), F8-T/BT@F8TPA<sub>fb</sub> (darker cyan), and F8TPA@TPABT<sub>fb</sub>@F8-T/BT<sub>s</sub> (yellow) particles. Solid lines in (d) and (e) represent measured data, dashed lines represent the exponential fits. f) Schematic and qualitative illustration of the polymer energy levels in the respective core-shell and core-shell-shell particles.

the first 20 min of the seed preparation. Both segments follow the typical function for particle growth at constant feed, where the diameter  $d$  scales with the cube root of the monomer conversion  $p$  ( $d \propto \sqrt[3]{p}$ ).<sup>[11]</sup> This demonstrates that during fed-batch core-shell particle formation, we have controlled growth of the shell onto the seed particles. This approach is universal and can also be applied for other conjugated polymer combinations (see Figures S4 for F8TPA@F8BT<sub>fb</sub> and Figure S5 for F8-T/BT@F8<sub>fb</sub> in the Supporting Information).

Besides the fed-batch dispersion polymerization, we also explore the seeded dispersion polymerization for CPP@CPP<sub>s</sub> (subscript s for seeded) core shell particle formation. For this purpose, we synthesize monodisperse core particles with diameters of about 580 nm from both F8TPA and F8-T/BT and use these particles as seeds in subsequent shell syntheses of the opposite polymer, respectively. To our surprise, an amount of 100  $\mu\text{mol}$  of M1 and M4 (to form the F8TPA shell) yields F8-T/BT@F8TPA<sub>s</sub> particles that hardly exhibit any shell growth. For comparison, in the fed-batch process, this amount of F8TPA monomers would have yielded a shell thickness of more than 200 nm. Repeating the shell growth step in a second seeded dispersion polymerization yields only a small increase in diameter of the F8-T/BT@F8TPA<sub>s</sub> particles (see Figure 1e, middle and Figure 1f). Polymerization and condensation of polymer chains onto the seed particles appears to be inhibited, due to the previously explained problem of heterocoagulation of the shell polymer. This phenomenon is substantiated by SEM displaying a rough surface of the particles suggesting aggregation of small particles to the seed particle surface rather than condensation of individual polymer

chains (see Figure S6a in the Supporting Information middle and right).

Despite observing only negligible shell growth by seeded dispersion polymerization, the presence of shell polymer is confirmed by the appearance of a significant absorption band at 380 nm together with fluorescence rising at 430 nm, both spectroscopic signatures can be assigned to the F8TPA shell in F8-T/BT@F8TPA<sub>s</sub> particles (see Figure S6b,c in the Supporting Information).

To investigate, whether heterocoagulation is specific to the F8TPA polymer as a shell, we invert the synthesis and produce F8TPA core particles, onto which we deposit the F8-T/BT shell (F8TPA@F8-T/BT<sub>s</sub>) (see Figure 1e, right). By contrast, F8-T/BT produced smooth particle shells that are controllable in their thickness (11.5 mmol L<sup>-1</sup> of monomers yield a 33 nm shell), suggesting that not only the polymer-polymer interactions but also the polymer-solvent interactions play a role in the shell formation; more specifically whether the shell forms through polymer condensation onto the seed-surface or via heterocoagulation (see Figure 1f).

Having now available two different synthetic pathways to produce smooth core-shell CPP@CPP, we wish to understand whether the seeded or fed-batch syntheses lead to different core-shell architectures. We hypothesize that the seeded dispersion polymerization leads to a clear interface between the core- and the shell-polymer, while the fed-batch process allows incorporation of residual core-monomers into shell-polymers yielding a gradient rather than a clearly separated polymer interface. The different core-shell architectures are difficult to resolve using optical imaging techniques, as there are energy

transfer phenomena between the core and shell polymers at play, obviating the clear resolution of this heterojunction. However, the energy transfer phenomena themselves could give insight into whether we have a clearly defined interface or a gradient between the two conjugated polymer phases.

We first record the absorption and emission spectra of the pure F8-T/BT and F8TPA polymers.

For absorption measurements, we dissolve the respective particles in tetrahydrofuran (THF), as otherwise absorption could not be recorded because the particles scatter strongly in the blue and near UV spectral range. F8TPA in THF displays maximum absorption at 380 nm. The F8TPA particles dispersed in *n*-propanol exhibit photoluminescence in the blue spectrum peaking at 430 nm ( $\lambda_{\text{ex}} = 390$  nm) (see Figure 2a). These spectral features of the F8TPA particles resemble those of structurally related TFB polymer.<sup>[39]</sup> The F8-T/BT solution in THF shows two absorption maxima at 320 and 510 nm. The red emission of an F8-T/BT particle dispersion in *n*-propanol is broad and peaks at 700 nm ( $\lambda_{\text{ex}} = 450$  nm) (see Figure 2a). Despite the slight structural difference, absorption and fluorescence spectra of F8-T/BT resemble the spectra of F8TBT, indicating that there is ample thiophene–benzothiadiazole–thiophene coupling also in F8-T/BT.<sup>[40]</sup> This knowledge of the optical properties of the individual polymers, allows us to individually excite the respective polymers for imaging by confocal microscopy. While confocal imaging allows clear assignment of the respective polymers and their emission colors to either the core or the shell of the particle, the area between the two polymers (clear interface or gradient) cannot be resolved (see Figure 2b). However, comparing the emission profiles of the core–shell particles with the pure polymer particles allows for some assessment of the interplay between core and shell polymers on the molecular level. We find that the emission of the F8-T/BT@F8TPA<sub>s</sub> particles, prepared by seeded dispersion polymerization, resembles a linear combination of the emission spectra of the pure F8TPA and F8-T/BT polymers (see Figure 2c and Figure S7 (Supporting Information)). The same is true for the inverse case of F8TPA@F8-T/BT<sub>s</sub> particles; however, the red emission is shifted bathochromically probably due to enhanced crystallinity in the F8-T/BT core. The separated spectral features indicate a sharp separation of the core and the shell polymer, as energy transfer phenomena will only occur over a very short distance and therefore not contribute significantly to the emission spectrum (see Figure 2c, schematic illustration). Furthermore, misalignment of the dipoles at the interface could inhibit Förster resonance energy transfer. This is different for the F8-T/BT@F8TPA<sub>fb</sub> particles, prepared via fed-batch dispersion polymerization, where the blue F8TPA emission band is bathochromically shifted by 23 nm and there is some weak emission in the green spectrum ( $\approx 560$  nm), which could originate from M2 monomers that have become incorporated into the F8TPA shell. This observation hints at mixed polymer species and a gradual transition from the core to the shell polymer (see Figure 2c, schematic illustration). To further corroborate our hypothesis of a sharp interface in core–shell particles prepared by seeded- and a polymer composition gradient in the fed-batch dispersion polymerization, we perform time correlated single photon counting (TCSPC) experiments with the core–shell particles (see Figure 2d). We determine the average photoluminescence lifetimes  $\tau_{\text{av}}$  of the F8TPA

**Table 1.** F8TPA donor emission. Fluorescence lifetimes  $\tau_1$  and  $\tau_2$  and the average lifetime  $\tau_{\text{av}}$  in different core–shell CPP architectures obtained by biexponential fitting ( $I = A_1 \exp(-t/\tau_1 \times t) + A_2 \exp(-t/\tau_2 \times t)$ ).

Particles	$\tau_1$ [ns]	$\tau_2$ [ns]	$\tau_{\text{av}}$ [ns]
F8-T/BT@F8TPA <sub>s</sub>	0.69	1.48	1.03
F8-T/BT@F8TPA <sub>fb</sub>	0.47	1.34	0.60

(donor) using a biexponential fit to the decays (see Table 1 and Figure S8a,b (Supporting Information)). The fluorescence lifetime of the F8TPA emission is shorter in the particles prepared via fed-batch (F8-T/BT@F8TPA<sub>fb</sub>:  $\tau_{\text{av}} = 0.60$  ns) than in the core–shell particles prepared via seeded dispersion polymerization (F8-T/BT@F8TPA<sub>s</sub>:  $\tau_{\text{av}} = 1.03$  ns). We attribute this shortened fluorescence lifetime to energy transfer from the F8TPA shell to the F8-T/BT core, which is more efficient and therefore faster across the polymer gradient compared to a sharp large-gap interface.<sup>[41,42]</sup>

The opposite trend is evident for the average photoluminescence lifetimes  $\tau_{\text{av}}$  of the F8-T/BT (acceptor) polymer in the respective core–shell architecture (see Figure 2e, Table 2 and Figure S8c–f (Supporting Information)). Pure F8-T/BT particles exhibit  $\tau_{\text{av}} = 0.373$  ns, which becomes longer in F8-T/BT@F8TPA particles, because the emission is further fed by energy transfer coming from the F8TPA donor. In the “fed-batch” F8-T/BT@F8TPA<sub>fb</sub> particles the F8-T/BT acceptor emission is longer ( $\tau_{\text{av}} = 1.30$  ns) compared to the “seeded” F8-T/BT@F8TPA<sub>s</sub> particles ( $\tau_{\text{av}} = 0.85$  ns). While the polymer gradient F8-T/BT@F8TPA<sub>fb</sub> enables fast depopulation of the pure F8TPA donor polymer, the transport along the gradient and emission from the F8-T/BT acceptor takes longer than in the case of the abrupt interface between F8TPA donor and F8-T/BT acceptor in F8-T/BT@F8TPA<sub>s</sub> particles. To substantiate this claim, we synthesize a core–shell–shell particle to control the composition between the F8TPA donor and F8-T/BT acceptor polymers. The shell between the donor and acceptor polymers is composed of monomers M2 and M4 to mimic a potentially occurring coupling step yielding the gradient in the fed-batch dispersion polymerization (see Figure 2f and Figure 3a,b).<sup>[43–45]</sup> This TPABT interlayer is produced following the fed-batch procedure, while the outermost shell is deposited after purification of the F8TPA@TPABT<sub>fb</sub> core–shell particles in a seeded dispersion polymerization yielding F8TPA@TPABT<sub>fb</sub>@F8-T/BT<sub>s</sub> particles. The individual polymers in this core–shell–shell all-conjugated polymer particles can be resolved via confocal

**Table 2.** F8-T/BT acceptor emission. Fluorescence lifetimes  $\tau_1$  and  $\tau_2$  and the average lifetime  $\tau_{\text{av}}$  in different core–shell CPP architectures obtained by biexponential fitting ( $I = A_1 \exp(-t/\tau_1 \times t) + A_2 \exp(-t/\tau_2 \times t)$ ). Photoluminescence quantum yields  $\Phi$  of F8-T/BT in the respective particles ( $\lambda_{\text{ex}}(\text{F8-T/BT}) = 490$  nm,  $\lambda_{\text{ex}}(\text{core-shell-shell}) = 390$  nm).

Particles	$\tau_1$ [ns]	$\tau_2$ [ns]	$\tau_{\text{av}}$ [ns]	$\Phi$ [%]
F8-T/BT	0.18	2.75	0.37	3.7
F8-T/BT@F8TPA <sub>s</sub>	0.38	2.89	0.85	1.0
F8TPA@TPABT <sub>fb</sub> @F8-T/BT <sub>s</sub>	0.54	2.10	0.96	3.1
F8-T/BT@F8TPA <sub>fb</sub>	0.33	3.53	1.31	1.2

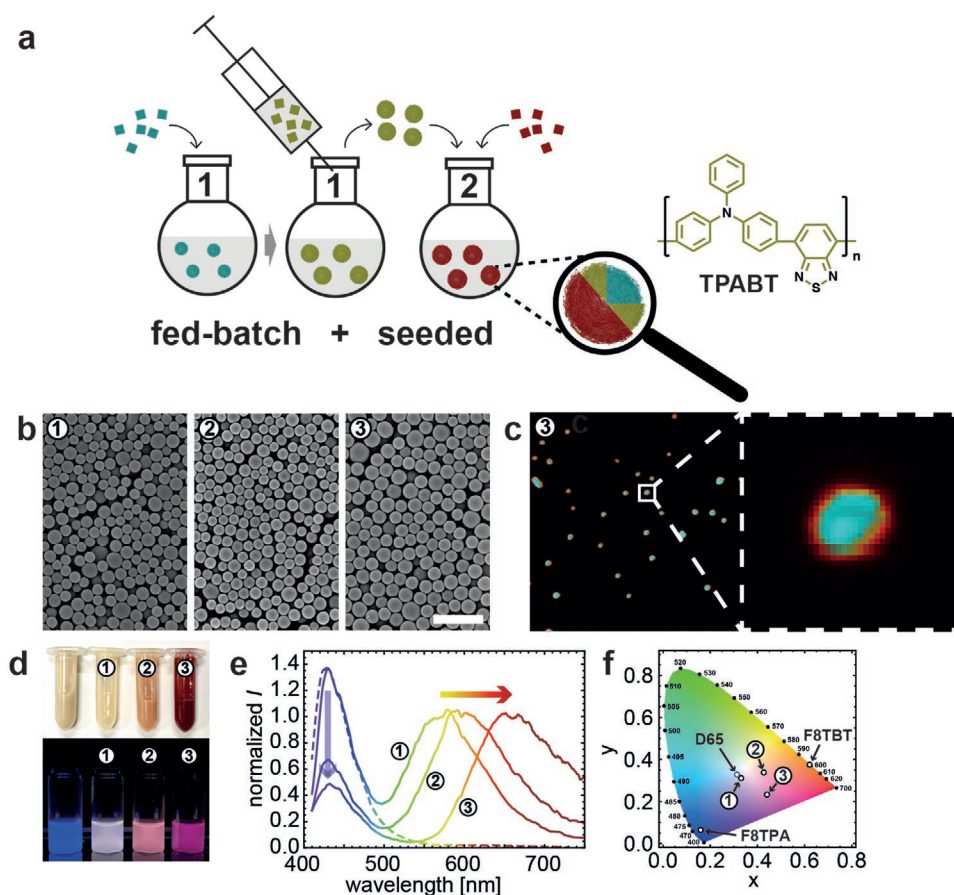


**Figure 3.** Synthesis of white emitting core-shell CPP and core-shell-shell CPP. a) Schematic illustration of the combined fed-batch and seeded dispersion polymerization resulting in core-shell-shell CPP and chemical structure of TPABT synthesized from monomers M2 and M4. b) SEM images of F8TPA@TPABT<sub>fb</sub> (①) and F8TPA@TPABT<sub>fb</sub>@F8-T/BT<sub>s</sub> (②,③) obtained with 9.2 and 18.4 mmol L<sup>-1</sup> F8-T/BT monomers respectively. Scale bar represents 2 μm. c) CLSM data of the F8TPA@TPABT@F8-T/BT CPP (③). d) Dispersions of pure F8TPA particles (left) and particles ①–③ in *n*-propanol. Photographs of the dispersions at room light (top) and of the fluorescence with an excitation at 365 nm (bottom). e) Fluorescence spectra of particle dispersions ①–③ in *n*-propanol and of a solution of particles ① in THF (dashed line).  $\lambda_{\text{ex}}$  is 390 nm. f) CIE diagram showing the human color perception resulting from the fluorescence spectra of particle dispersions ①–③ and of pure F8TPA and F8-T/BT particles in *n*-propanol. D65 is a CIE Standard Illuminant that corresponds to the natural average daylight in western and northern Europe. It marks the white point and represents the white light emission of an ideal emitter (black body) at about 6500 K.

microscopy (see Figure 3c). The average fluorescence lifetime ( $\tau_{\text{av}} = 0.96$  ns) is between those of the F8-T/BT@F8TPA particles prepared via fed-batch or seeded dispersion polymerization, confirming that energy transfer along the gradient requires more time than across a single distinct interface (see Figure 2e and Table 2).

Having understood the morphology and energy transfer phenomena, which can arise in accordance with the different synthetic pathways, we set out to produce white light emitting single conjugated polymer particles. Due to the fed-batch dispersion polymerization we are able to adjust the shell thickness of the broadband TPABT emitter and thus the intensity of its respective emission band in the fluorescence spectrum. Increasing the TPABT shell thickness in the fed-batch synthesis of F8TPA@TPABT<sub>fb</sub> particles leads to a controllable shift in the acceptor emission. Increasing the shell thickness of TPABT leads to a systematic shift towards the yellow spectrum, which can be understood by assuming proceeding consumption of

residual M1 and M4 monomers (from the F8TPA core) and growing purity of the TPABT polymer for increasing shell thickness. This gradient in polymer composition entails a bathochromic shift as energy will be transferred along the gradient to the purest TPABT polymers due their lowest bandgap, where emission will take place (see Figure 3d,e③). Attachment of an additional shell of F8-T/BT to these particles via seeded dispersion polymerization yields F8TPA@TPABT<sub>fb</sub>@F8-T/BT<sub>s</sub> particles and further bathochromic shift of the acceptor emission into the red spectrum (see Figure 3d,e②,③). This allows us to control the ratio of blue to yellow and red emission and we find white light fluorescence for F8TPA@TPABT<sub>fb</sub> particles ① (see Figure 3d). To quantify the emission color, we determine the chromaticity coordinates  $x$  and  $y$  for the CIE 1931 color space from the emission spectra of our F8TPA@TPABT<sub>fb</sub> particles. We can reach point D65 in the CIE system, corresponding to the natural average daylight in western and northern Europe (see Figure 3f and Table S4 (Supporting Information)).

### 3. Conclusion

In conclusion, we have presented monodisperse core–shell and core–shell–shell particles, where we have control over the precise energy transfer cascade. In the future, our synthetic toolbox approach can be used to adjust conjugated polymer particles precisely to the respective application. The inherent energy transfers within the particles could be advantageous in order to achieve large Stokes shifts for advanced bioimaging techniques or allow white light or multimodal laser emission from individual whispering gallery mode particles. Since the particles are monodisperse they could be applied for self-assembled organic photonics and optoelectronics enabling new device geometries and fabrication techniques.

### Supporting Information

Supporting Information is available from the Wiley Online Library or from the author.

### Acknowledgements

The authors thank Janina Hald for support with particle synthesis, Dr. Konstantin Sparrer and Dr. Markus Lamla for support with Confocal Microscopy (all at Ulm University). The authors acknowledge funding by the BMBF via a NanoMatFutur AktiPhotoPol (13N13522) research group. Open access funding enabled and organized by Projekt DEAL.

### Conflict of Interest

The authors declare no conflict of interest.

### Data Availability Statement

The data that support the findings of this study are available from the corresponding author upon reasonable request.

### Keywords

conjugated polymer particles, core–shell particles, white light emission

Received: March 25, 2021

Published online:

- [1] D. Tuncel, H. V. Demir, *Nanoscale* **2010**, *2*, 484.  
 [2] J. Pecher, S. Mecking, *Chem. Rev.* **2010**, *110*, 6260.  
 [3] C. Wu, D. T. Chiu, *Angew. Chem., Int. Ed.* **2013**, *52*, 3086.  
 [4] X. Feng, X. Ding, D. Jiang, *Chem. Soc. Rev.* **2012**, *41*, 6010.  
 [5] K. Müller, M. Klapper, K. Müllen, *Macromol. Rapid Commun.* **2006**, *27*, 586.  
 [6] M. Antonietti, K. Landfester, *Prog. Polym. Sci.* **2002**, *27*, 689.  
 [7] J. Pecher, J. Huber, M. Winterhalder, A. Zumbusch, S. Mecking, *Biomacromolecules* **2010**, *11*, 2776.  
 [8] C. Szymanski, C. Wu, J. Hooper, M. A. Salazar, A. Perdomo, A. Dukes, J. McNeill, *J. Phys. Chem. B* **2005**, *109*, 8543.  
 [9] T. Adachi, L. Tong, J. Kuwabara, T. Kanbara, A. Saeki, S. Seki, Y. Yamamoto, *J. Am. Chem. Soc.* **2013**, *135*, 870.

- [10] A. I. J. C. Kuehne, M. C. Gather, J. Sprakel, *Nat. Commun.* **2012**, *3*, 1088.  
 [11] S. Ciftci, A. J. C. Kuehne, *Macromolecules* **2015**, *48*, 8389.  
 [12] L. Parrenin, C. Brochon, G. Hadziioannou, E. Cloutet, *Macromol. Rapid Commun.* **2015**, *36*, 1816.  
 [13] N. Anwar, A. Rix, W. Lederle, A. J. C. Kuehne, *Chem. Commun.* **2015**, *51*, 9358.  
 [14] C. Wu, C. Szymanski, Z. Cain, J. McNeill, *J. Am. Chem. Soc.* **2007**, *129*, 12904.  
 [15] C. Wu, B. Bull, C. Szymanski, K. Christensen, J. McNeill, *ACS Nano* **2008**, *2*, 2415.  
 [16] A. J. C. Kuehne, M. C. Gather, *Chem. Rev.* **2016**, *116*, 12823.  
 [17] A. Mikosch, S. Ciftci, A. J. C. Kuehne, *ACS Nano* **2016**, *10*, 10195.  
 [18] J. B. Ten Hove, J. Appel, J. M. Van Den Broek, A. J. C. Kuehne, J. Sprakel, *Small* **2014**, *10*, 957.  
 [19] S. Ciftci, A. Mikosch, B. Haehnle, Ł. Witczak, A. J. C. Kuehne, *Chem. Commun.* **2016**, *52*, 14222.  
 [20] P. Howes, M. Green, A. Bowers, D. Parker, G. Varma, M. Kallumadil, M. Hughes, A. Warley, A. Brain, R. Botnar, *J. Am. Chem. Soc.* **2010**, *132*, 9833.  
 [21] S. Li, X. Shen, Q. H. Xu, Y. Cao, *Nanoscale* **2019**, *11*, 19551.  
 [22] T. Repenko, A. Rix, A. Nedilko, J. Rose, A. Hermann, R. Vinokur, S. Moli, R. Cao-Milàn, M. Mayer, G. von Plessen, A. Fery, L. De Laporte, W. Lederle, D. N. Chigrin, A. J. C. Kuehne, *Adv. Funct. Mater.* **2018**, *28*, 1705607.  
 [23] C. Wu, C. Szymanski, J. McNeill, *Langmuir* **2006**, *22*, 2956.  
 [24] D. C. Sundberg, Y. G. Durant, *Polym. React. Eng.* **2003**, *11*, 379.  
 [25] J. Stubbs, O. Karlsson, J. E. Jönsson, E. Sundberg, Y. Durant, D. Sundberg, *Colloids Surf., A* **1999**, *153*, 255.  
 [26] D. C. Sundberg, A. P. Casassa, J. Pantazopoulos, M. R. Muscato, B. Kronberg, J. Berg, *J. Appl. Polym. Sci.* **1990**, *41*, 1425.  
 [27] H. F. Hernandez García, *Multi Scale Simulation of Heterophase Polymerization – Application to the Synthesis of Multicomponent Colloidal Polymer Particles*, Universität Potsdam, Institutional Repository of the Potsdam University (Dissertation) **2008**.  
 [28] L. C. Hsiao, S. Pradeep, *Curr. Opin. Colloid Interface Sci.* **2019**, *43*, 94.  
 [29] D. Nguyen, E. Duguet, E. Bourgeat-Lami, S. Ravaine, *Langmuir* **2010**, *26*, 6086.  
 [30] M. C. Gather, A. Köhnen, K. Meerholz, *Adv. Mater.* **2011**, *23*, 233.  
 [31] C. Kim, Y. J. Gwon, J. Kim, T. S. Lee, *Polym. Chem.* **2018**, *9*, 5671.  
 [32] V. Revuri, K. Cherukula, M. Nafujjaman, K. J. Cho, I. K. Park, Y. K. Lee, *ACS Appl. Nano Mater.* **2018**, *1*, 662.  
 [33] A. Wagh, F. Jyoti, S. Mallik, S. Qian, E. Leclerc, B. Law, *Small* **2013**, *9*, 2129.  
 [34] N. Miyaura, A. Suzuki, *Chem. Rev.* **1995**, *95*, 2457.  
 [35] B. Haehnle, M. Lamla, K. M. J. Sparrer, M. C. Gather, A. J. C. Kuehne, *Adv. Opt. Mater.* **2021**, *9*, 2001553.  
 [36] J. S. Song, F. Tronc, M. A. Winnik, *J. Am. Chem. Soc.* **2004**, *126*, 6562.  
 [37] W. Yang, R. A. Hutchinson, *Macromol. React. Eng.* **2016**, *10*, 71.  
 [38] M. Zhang, R. A. Hutchinson, *Macromol. React. Eng.* **2018**, *12*, 1.  
 [39] W. Renzi, N. J. A. Cordeiro, H. de Santana, M. F. Costa, M. A. T. da Silva, E. Laureto, J. L. Duarte, *Synth. Met.* **2018**, *236*, 24.  
 [40] L. P. Lu, C. E. Finlayson, D. Kabra, S. Albert-Seifried, M. H. Song, R. W. A. Havenith, G. Tu, W. T. S. Huck, R. H. Friend, *Macromol. Chem. Phys.* **2013**, *214*, 967.  
 [41] C. V. Kumar, M. J. Novak, K. R. Benson, C. Baveghems, V. K. Thilakarathne, B. S. Stromer, F. M. Ross, *RSC Adv.* **2015**, *5*, 72416.  
 [42] S. Kushida, D. Braam, T. D. Dao, H. Saito, K. Shibasaki, S. Ishii, T. Nagao, A. Saeki, J. Kuwabara, T. Kanbara, M. Kijima, A. Lorke, Y. Yamamoto, *ACS Nano* **2016**, *10*, 5543.  
 [43] A. S. D. Sandanayaka, K. Matsukawa, T. Ishi-I, S. Mataka, Y. Araki, O. Ito, *J. Phys. Chem. B* **2004**, *108*, 19995.  
 [44] S. Liu, H. Zhang, Y. Li, J. Liu, L. Du, M. Chen, R. T. K. Kwok, J. W. Y. Lam, D. L. Phillips, B. Z. Tang, *Angew. Chem., Int. Ed.* **2018**, *57*, 15189.  
 [45] C. Liu, L. Liu, Y. Liu, Z. Dang, C. Li, *Catal. Sci. Technol.* **2021**, *11*, 1862.